INSTITUTE OF PLASMA PHYSICS

NAGOYA UNIVERSITY

RESEARCH REPORT

NAGOYA, JAPAN

Observation of Ion Acoustic Wave by Microwave Scattering Method

Atsushi Mase*, Takumi Yamamoto*,
and Takashige Tsukishima*

IPPJ-172 August 1973

Further communication about this report is to be sent to the Research Information Center, Institute of Plasma Physics, Nagoya University, Nagoya, JAPAN.

* Faculty of Engineering, Nagoya University, Nagoya

Abstract

An ion acoustic wave in a current carrying plasma is studied by microwave scattering method. A technique of incoherent scattering of electromagnetic wave of f_i = 35 GHz by ion acoustic waves of f = 20 — 70 kHz is described. A dispersion relation and the intensity distribution in k-space of the ion acoustic wave is determined from the angular distribution of the scattered wave. A spatial evolution of the ion acoustic waves along the tube axis is also observed. The observed spatial growth rates are compared with calculated values which take account of both linear and non-linear growth rates. A good agreement is obtained when the non-linear effect is assumed as mainly due to the ion-trapping.

I. Introduction

The importance of using incoherent scattering of electromagnetic wave from plasma as a diagnostic tool has been widely recognized. This technique is a powerful tool for diagnosing high temperature plasmas; the plasma parameters such as the electron density and temperature can be measured without disturbing the plasmas, and the dynamic form factors of the turbulent plasmas (such as the energy distribution of a turbulence in the ω-k space) can be also detected. The microwave scattering is especially superior to the laser scattering for detecting the low frequency waves which are relevant to the anomalous diffusions and conductivities. Microwave scattering from a variety of laboratory plasmas has been observed.[1-3]

We report here on the experimental results of an R-band (35 GHz) microwave scattering from ion acoustic waves excited externally in a mercury positive column.[4] The receiver system consists of a frequency based correlator,[5] and has a frequency resolution of 3 kHz. A spatial resolution of about 2 cm is also achieved by using a dielectric lens. With this non-perturbing probe the properties of the ion acoustic waves are studied and the plasma parameters are determined. A dispersion relation and the intensity distribution in k-space of the ion acoustic wave is determined from the angular distribution of the scattered wave. A spatial evolution of the ion acoustic waves along the tube axis is also observed. The observed spatial growth rates are compared

with calculated values which take account of both linear and non-linear growth rates. A good agreement is obtained when the non-linear effect is assumed as mainly due to the ion-trapping. The experimental arrangement is described in Sec.II. The experimental results and discussions are given in Sec.III. In Sec.IV, the calculation of the spatial evolution of the ion acoustic wave is described and compared with the measured values. The section V summarizes this study.

II. Experimental Arrangement

The experimental arrangement is shown schematically in Fig.1. The plasma is produced in a glass tube with 5 cm i.d. and 45 cm long which has a mercury bath. The discharge current I_d is varied from 0.1 A to 0.9 A. Then, the mean electron density N for I_d=0.9 A is about 1.4×10^{10} cm^{-3}. The electron temperature T_e is measured with a Langmuir probe and a value of $T_e \simeq 1.3$ eV is obtained. Thus, the ion plasma frequency $f_{pi} \simeq 1.7$ MHz, and the electron Deby length $\lambda_D \simeq 7.1 \times 10^{-3}$ cm. The ion temperature T_i is not measured directly in the experiment. As will be shown later, the value of T_i is of the order of 0.1 eV. The mercury vapor pressure p is controlled by the room temperature, and has a value of $p \simeq 2.5 \times 10^{-3}$ torr. In this plasma the electrons are drifting along the tube axis (this is taken as z-axis, hereafter) due to the axial electric field E_z. A value of $E_z \simeq 0.16$ V/cm is obtained by measuring the average potential difference between

two probes located along the tube axis.

The ion acoustic waves are excited via an asterisk grid, to which a continuous sinusoidal wave of frequency $\omega/2\pi$ from an oscillator is applied. The grid is located 16 cm distant from the cathode.

A microwave of the frequency $\omega_i/2\pi$ =35 GHz is launched through the transmitter horn and focused on the discharge tube by using a dielectric lens. The transverse width of the incident beam is about 2 cm on the tube axis, while the intensity is nearly constant along the beam direction over the tube diameter. The electric field vector E_i is perpendicular to the tube axis. Both the discharge tube and the receiver horn are made rotatable around an axis paralell to E_i, located at the focal point of the incident beam. The discharge tube is movable along its axis, too, in order for the illuminating position to be scaned along the tube axis. The plasma column is in the far field of both horns. The scattered signal picked up by the receiver horn is detected by a homodyne svstem. In order to obtain a good signal to noise ratio at the receiver output, a frequency based correlator with 3 kHz i.f. band width is usèd.

For the present experimental condition of $\omega_i \gg \omega$, the scattered waves with frequencies $\omega_s = \omega_i + \omega$ and $\omega_s' = \omega_i - \omega$ enter into the receiver horn as shown in Fig.1. Thus, the input field to the crystal detector is a linear sum of the two satellites, $E_s\cos(\omega_s t + \varphi_s)$ and $E_s'\cos(\omega_s' t + \varphi_s')$, the strayed incident field $E_i\cos(\omega_i t + \varphi_i)$ and the local field $E_l\cos(\omega_i t + \varphi_l)$. The outputs

of the two crystals are, then, given by

$$\begin{aligned} e_A &= A\,[\,E_s\cos(\omega_s t+\varphi_s)+E_s'\cos(\omega_s' t+\varphi_s') \\ &\quad +E_l\cos(\omega_i t+\varphi_l)+E_i\cos(\omega_i t+\varphi_i)]^2\ , \\ e_B &= B\,[\,E_s\cos(\omega_s t+\varphi_s)+E_s'\cos(\omega_s' t+\varphi_s') \\ &\quad -E_l\cos(\omega_i t+\varphi_l)+E_i\cos(\omega_i t+\varphi_i)]^2\ , \end{aligned} \tag{1}$$

provided that the crystals have the square characteristic, where A and B are the conversion gain factor of the crystals, and φ_s, φ_s', φ_l and φ_i are the phase components of the each electric field. The i.f. outputs of frequency ω are given by

$$\begin{aligned} e_A' &= A'[\,E_sE_l\cos(\omega t+\varphi_s-\varphi_l)+E_s'E_l\cos(\omega t+\varphi_l-\varphi_s') \\ &\quad +E_sE_i\cos(\omega t+\varphi_s-\varphi_i)+E_s'E_i\cos(\omega t+\varphi_i-\varphi_s')]\ , \\ e_B' &= B'[\,E_sE_l\cos(\omega t+\varphi_s-\varphi_l)+E_s'E_l\cos(\omega t+\varphi_l-\varphi_s') \\ &\quad -E_sE_i\cos(\omega t+\varphi_s-\varphi_i)+E_s'E_i\cos(\omega t+\varphi_i-\varphi_s')]\ , \end{aligned} \tag{2}$$

where A' and B' are constants. When the condition $E_l \gg E_i$ is satisfied, we obtain the following correlator output P_r,

$$P_r = \overline{|e_A' \times e_B'|} = \frac{A'B'}{2}E_l^2\,(\,E_s^2+E_s'^2+2E_sE_s'\cos\phi\,)\ , \tag{3}$$

where upper bar denotes the time average, and $\phi = \varphi_s+\varphi_s'-2\varphi_l$. The value of ϕ can be controlled by the phase shifter shown in

Fig.1. Note that P_r becomes independent of ϕ when only either of the two satellites are to be received.

III. Experimental Results

A. The dispersion relation

Figure 2 shows the observed correlator output P_r versus the scattering angle θ_s for the normal incidence to the tube axis, i.e. $\theta_d=0$. Here, θ_d is defined as the rotation angle of the discharge tube from the position where the tube axis is normal to the direction of the incident beam. The vertical bars shown in Fig.2 are more or less of the type of error bar of the measurement, and the variations of P_r are buried in these bars even when the phase ϕ is varied from 0 to 2π rad. for each θ_s. Thus, refering to Eq.(3), we may conclude that the observed peaks are due to either E_s or E_s'. Since the corresponding matching conditions for the wave vectors are given by

$$\begin{aligned} \mathbb{K}_s &= \mathbb{K}_i + \mathbb{k} \quad , \\ \mathbb{K}_s' &= \mathbb{K}_i - \mathbb{k} \quad , \end{aligned} \tag{4}$$

where $K_s = \omega_s/c$, $K_s' = \omega_s'/c$, c is the light velocity and $\mathbb{k}$ is the wave vector of the ion acoustic wave, the peak for $\theta_s>0$ is identified with the upper satellite at ω_s and that for $\theta_s<0$ with the lower satellite at ω_s'. As is illustrated in Fig.3, these satellites are due to the ion acoustic waves propagating toward

the anode at the angles $\pm \theta_s/2$ from the tube axis. Hence the correlator output P_r will be taken for the scattered power P_s by a single wave, hereafter.

The similar measurements were repeated for varying ω and for the two scattering regions, namely, one in the anode side and the other in the cathode side as viewed from the exciting grid. The waves in the anode side are propagating against the ion drift, while those in the cathode side are propagating along the ion drift. Since $K_i \simeq K_s \simeq K_s'$ in the present experiment, the value of k can be calculated by

$$k = 2K_i \sin(\theta_s/2) \quad , \tag{5}$$

with θ_s yielding the peak value of P_r.

The values of k thus obtained are plotted against ω in Fig.4, where the circles and dots stand for the waves propagating along and against the ion drift, respectively. In the presence of the ion drift V_i, the phase velocity v_p in the low frequency region is given by

$$v_p = \omega/k = c_s \pm V_i \cos(\theta_s/2) \quad , \tag{6}$$

where $c_s=(T_e/m_i)^{1/2}$ is the intrinsic ion acoustic speed, T_e is the electron temperature in energy unit, and m_i is the mass of an ion. From Fig.4 and Eq.(6), we obtain $v_{p+}=c_s+V_i=9.1\times10^4$ cm/sec and $v_{p-}=c_s-V_i=6.9\times10^4$ cm/sec. Hence we have $V_i=1.1\times10^4$ cm/sec and $c_s=8.0\times10^4$ cm/sec, yielding $T_e=1.3$ eV. This value of T_e agrees with that measured with a Langmuir probe. Note that since

$\cos(\theta_s/2) \simeq 0.95$, even for f=60 kHz, the error introduced in k by replacing $V_i \cos(\theta_s/2)$ by V_i in Eq.(6) is less than 1%.

In Fig.5 is shown the wave number versus the amplitude of the exciting signal, V_{ext}. Since k is almost independent of V_{ext}, the effect of the ballistic mode is considered to be small here.[6]

B. Distribution in k-space of ion acoustic wave

In order to see the intensity distribution of the ion acoustic wave as a function of the zenithal angle α as measured from the tube axis, the discharge tube is rotated while the receiver horn is located at the fixed θ_s giving the peak P_r for the normal incidence. Figure 6 shows some examples of the intensity distributions of the waves in the anode side. It is seen that the wave intensity shows the maximum at $\alpha=0$, as is expected. The observed angular spread for low frequency is wider than that for high frequency, and both exceed the instrumental broadening. This may be partly due to the fact that the diameter of the exciting grid becomes comparable with the wavelength for the low frequency wave.

C. The spatial evolution of the ion acoustic wave

As has been shown in the previous section, the ion acoustic wave with k parallel to the tube axis (i.e. $\alpha=0$) is most intensive. In order to measure the spatial evolution of this wave along the z axis, the discharge tube is moved along its axis. Both θ_s and θ_d are fixed at appropriate values for a given ω,

so as to satisfy the matching condition $\mathbb{K}_s = \mathbb{K}_i + \mathbb{k}$.

Figure 7 shows the scattered power $P_s(z)$ versus the illuminating position z as measured from the exciting grid toward the anode. The wave with f>50 kHz grows initially with z. This is because the growth rate due to the electron drift exceeds other damping processes. As the wave propagates, the amplitude begins to saturate and even attenuates with further increase of z. A phenomenological analysis of the cause of the nonlinear saturation is developed in the next section.

IV. Analysis of the Spatial Evolution of the Ion Acoustic Wave

For simplicity, a plane monochromatic wave is considered. The wave amplitude $\Phi(z)$ of the potential fluctuation may be expressed in W.K.B. approximation as follows,

$$\Phi(z) = \Phi(0)\exp\left[\int_0^z k_i(z)dz\right] , \qquad (7)$$

provided that $|k_i| \ll |k|$, where k_i is a sum of a linear growth rate k_{iL} and a nonlinear growth rate k_{iNL}. A theoretical expression of k_{iL} has been derived from the dispersion relation of the ion acoustic wave in a current carrying plasma,[7] that is,

$$k_{iL} = - \frac{\nu_{in}}{2c_s} - \frac{\pi^{3/2}}{\sqrt{2}} f \frac{c_s}{(c_s - V_i)^2}$$

$$\times \left\{ \theta^{3/2} \exp\left(- \frac{\theta}{2}\right) + \rho^{1/2} \left(1 - \frac{V_e + V_i}{c_s}\right) \right\} \quad , \quad (8)$$

provided that $T_e \gg T_i$, where ν_{in} is the ion-neutral collision frequency, $\theta = T_e/T_i$, $\rho = m_e/m_i$, m_e is the electron mass and V_e is the electron drift velocity.

For the ion-trapping, the nonlinear growth rate is given by[8,9]

$$k_{iNL} \simeq \delta k \, [e \Phi(z)/T_e]^{1/2} \quad , \quad (9)$$

where δ is a numerical factor of the order of 10^{-1}. From Eqs. (8) and (9), and noting that $P_s(z) \propto \Phi^2(z)$, we have

$$\frac{1}{2} \ln \left[\frac{P_s(z)}{P_s(0)}\right] = k_{iL} z - \delta k \left(\frac{e \Phi(0)}{T_e}\right)^{1/2} \int_0^z \left[\frac{P_s(z)}{P_s(0)}\right]^{1/4} dz \quad , \quad (10)$$

Note that even for small z, the net growth rate includes the nonlinear term.

By comparing Eq.(10) with the observed values of $P_s(z)/P_s(0)$ in the range of small z, one can determine k_{iL} and $k_{iNL}(0)$. The values of k_{iL} so obtained for various frequencies are shown in Table I, together with those calculated from Eq.(8). A satisfactory agreement between the two values is obtained. In calculating the Eq.(8), the following values are used: $\nu_{in} = 7.2 \times 10^4$ sec^{-1}, $T_e/T_i = 13$ ($T_i = 0.1$ eV for $T_e = 1.3$ eV), $V_i = 1.1 \times 10^4$ cm/sec and $V_e =$

1.05×10^7 cm/sec. These values are directly measured by the probe or scattering method, or estimated,[10,11] and reasonable for our plasma ($E/p \simeq 60$).

The solid lines shown in Fig.7 are calculated step by step from Eq.(10), using the value of k_{iL} and $k_{iNL}(0)$ determined above and by making use of the graphical integration. The value of $P_s(0)$ is determined by a smooth extrapolation of the experimental values.

The value of $k_{iNL}(0)$ determined above can be also compared with the electron density fluctuation $n(z)$ normalized to the average density N, and extrapolated to $z=0$ assuming $n^2(z) \propto P_s(z)$. The value of $n(z)$ is measured with the probe. The best fit is obtained for $\delta = 0.13$: namely with this value of δ we have $n(0)/N \simeq e\,\Phi(0)/T_e$.

Although the nonlinear effect due to the ion-trapping is consistent with the experimental results, there still remains a possibility of the effect of the nonlinear wave-wave coupling between the fundamental and second harmonic waves. The wave-wave coupling theory says that two waves exchange their energy each other as

$$\Phi_1^2(z) + \Phi_2^2(z) = \left\{\Phi_1^2(0) + \Phi_2^2(0)\right\} \exp(2k_{iL}z) \quad , \qquad (11)$$

where $\Phi_1(z)$ is the amplitude of the fundamental wave, $\Phi_2(z)$ is that of the second harmonic wave, and k_{iL} is the growth rate for the fundamental wave. In Fig.8, the intensity of the second harmonic wave is plotted on the basis of the energy conservation of Eq.(11),

assuming that the observed saturation of the fundamental wave is due to the generation of the harmonic wave. To be exact, the growth rate of the harmonic wave calculated from the Eq.(8) is larger than that of the fundamental wave. Therefore, we should have still larger value of $\bar{\Phi}_2^2(z)$ when the exact growth rate for the second harmonic wave was used. In the present experiment, the second harmonic wave is observed for V_{ext}=20 V. However its level is much smaller than that of Fig.8. Moreover, the characteristic figure of P_s v.s. z is not changed essentially even when the harmonic wave is not found. Thus, the effect of the wave-wave coupling may be small. Very recently, Wong et al[13] observed the saturation of the spatial evolution of the ion acoustic instability and explained its results with BGK mode with trapped electrons. In our experiment, however, the effective electron-electron collision frequency exceed the electron bounce frequency even at the maximum amplitude of ion acoustic wave. Thus, electron-trapping effect may be suppressed by the collisions.[14]

V. Concluding Remarks

In conclusion, we have obtained the followings.

(1) The ion acoustic waves with frequency of 20—70 kHz are excited on the mercury positive column, on which the microwave with frequency of 35 GHz is radiated through the dielectric lens. Then, the scattered wave is measured by means of the correlation technique. Microwave scattering system which has the spatial

resolution of about 2 cm and the frequency resolution of 3 kHz is achieved.

(2) From the angular distribution of the scattered waves, the dispersion relation is obtained for the waves propagating along the ion drift and along the electron drift. Thus the ion acoustic velocity and the ion drift velocity are determined. The ion acoustic velocity agrees well with that obtained by the probe measurement.

(3) The intensity distribution of ion acoustic waves in $\mathbb{k}$-space is measured. It is found that the wave with $\mathbb{k}$ parallel to the tube axis is most intensive.

(4) The experimental results of the spatial evolution is compared with the theoretical one which take account of both linear and nonlinear growth rates in W.K.B. approximation. From the best fit between the measured and calculated values, both growth rates are determined.

(5) The linear growth rate thus obtained agrees well with the theoretical value derived for a current carrying plasma.

(6) The values of the nonlinear growth rate are also reasonable when the nonlinear effect is assumed to be due to the ion-trapping. It is shown that the nonlinear effect due to the coupling between the fundamental and second harmonic waves is not important here.

Acknowledgements

The authors deeply appreciate Dr. N. Sato of Tohoku University for the discussions on the linear growth rate in a current carrying plasma. This work is supported in part by the Grant-in-Aid for Scientific Research from the Ministry of Education and also by the collaborating Research Program at Institute of Plasma Physics, Nagoya University, Nagoya.

References

1 V. Arunasalam, M. A. Heald, and J. Sinnis, Phys. Fluids 14, 1194 (1971). Other references for microwave scattering may be found in this paper and in Refs. 2 and 3.

2 L. D. Bollinger and H. Bohmer, Phys Fluids 15, 693 (1972).

3 I. P. Shakarofsky, A. K. Ghosh, and E. N. Almey, Plasma Phys. 14, 935 (1972).

4 For a brief report of one of these results, see A. Mase, T. Yamamoto, and T. Tsukishima, J. Phys. Soc. Japan 34, 1426 (1973).

5 T. Tsukishima and A. Mase, J. Phys. Soc. Japan 33, 276 (1972).

6 I. Alexeff, W. D. Jones, and K. Lonngren, Phys. Rev. Letters 21, 878 (1968).

7 N. Sato, A. Sasaki, K. Aoki, and Y. Hatta, Phys. Rev. Letters 19, 1174 (1967).

8 H. Ikezi, Y. Kiwamoto, K. Nishikawa, and K. Mima, Phys. Fluids 15, 1605 (1972).

9 A. Sleeper, J. Weinstock, and B. Bezzerides, Phys. Rev. Letters 29, 343 (1972). The value of k_{iNL} can be related to Γ in Eq.(9) of Ref.9, by $k_{iNL}=(k/\omega)\Gamma$, which reduces to $k_{iNL}\simeq 0.6\, k(e\Phi/T_e)^{1/2}$ when only a single mode exists. We have used the relations, $|\delta E_k|^2 \cong k^2\Phi^2$, $T_e/m_i \simeq \omega^2/k^2$, and $\lambda_D^2 = T_e/4\pi e^2 n$.

10 H. Tanaca, A. Hirose, and M. Koganei, Phys. Rev. 161, 94 (1967).

11 K. Kingdon and E. Lawton, Phys. Rev. 56, 215 (1939).

12 T. Ohnuma, T. Fujita, S. Ohnuki, Y. Nakamura, and S. Adachi, to be published in Phys. Rev. A, Aug. (1973).

13 A. Y. Wong, B. H. Quon, and B. H. Ripin, Phys. Rev. Letters 30, 1299 (1973).

14 K. Nishikawa and C. S. Wu, Phys. Rev. Letters 23, 920 (1969).

Figure Captions

Fig. 1 Schematic of the experimental apparatus.

Fig. 2 Received power versus the scattering angle θ_s.

Fig. 3 Relationships among the wave vectors for $\theta_s > 0$ and $\theta_s < 0$.

Fig. 4 Dispersion relations for the waves in the anode side and in the cathode side as viewed from the exciting grid.

Fig. 5 Wave numbers versus the amplitude of exciting signal.

Fig. 6 Scattered power versus the zenithal angle α from the tube axis. θ_s is fixed at the values giving the peak P_r: o $\theta_s > 0$, o $\theta_s < 0$.

Fig. 7 Scattered power versus the distance z from the exciting grid toward the anode.

Fig. 8 Spatial evolution of the fundamental wave (60 kHz), and the corresponding amplitude of the second harmonic wave calculated from Eq. (11).

Table I. The values of k_{iL}, $e\Phi(0)/T_e$ and $n(0)/N$ for various values of frequency f. The value of $e\Phi(0)/T_e$ is determined from $k_{iNL}(0)$ with $\delta = 0.13$. Normalized density fluctuation $n(0)/N$ is measured with the probe.

f(kHz)	k_{iL}(measured)	k_{iL}(calculated)	$e\Phi(0)/T_e$	n(0)/N
30	$-0.15\ cm^{-1}$	$-0.14\ cm^{-1}$	0.09	
50	$+0.09\ cm^{-1}$	$+0.075\ cm^{-1}$	0.025	
60	$0.19\ cm^{-1}$	$0.18\ cm^{-1}$	0.025	0.02
70	$0.30\ cm^{-1}$	$0.29\ cm^{-1}$	0.008	0.01

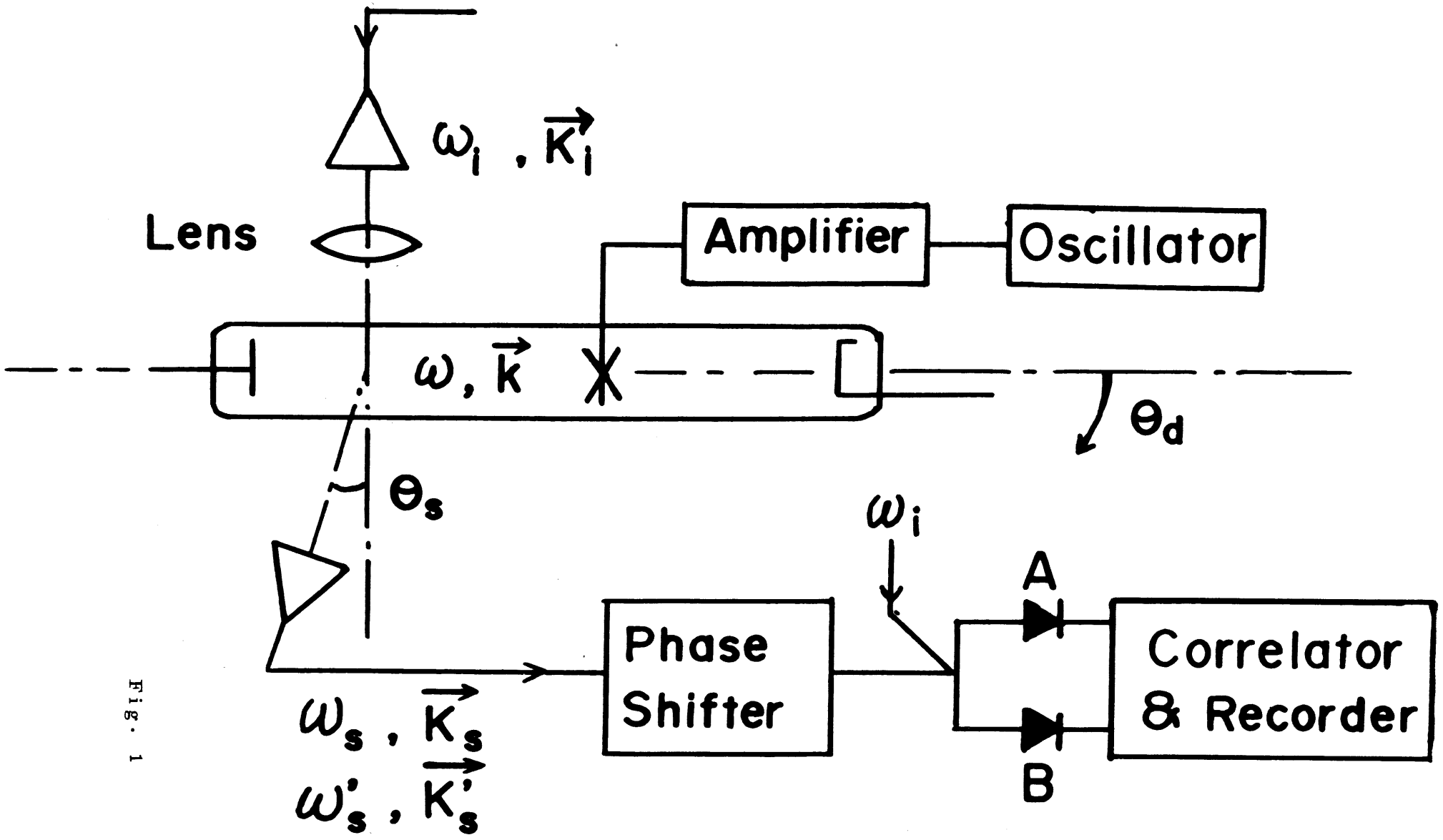
ω_i , $\vec{K}_i$
Lens
Amplifier
Oscillator
ω, $\vec{k}$
θ_d
θ_s
ω_i
A
Phase Shifter
Correlator & Recorder
B
ω_s , $\vec{K}_s$
ω_s' , $\vec{K}_s'$

Fig. 1

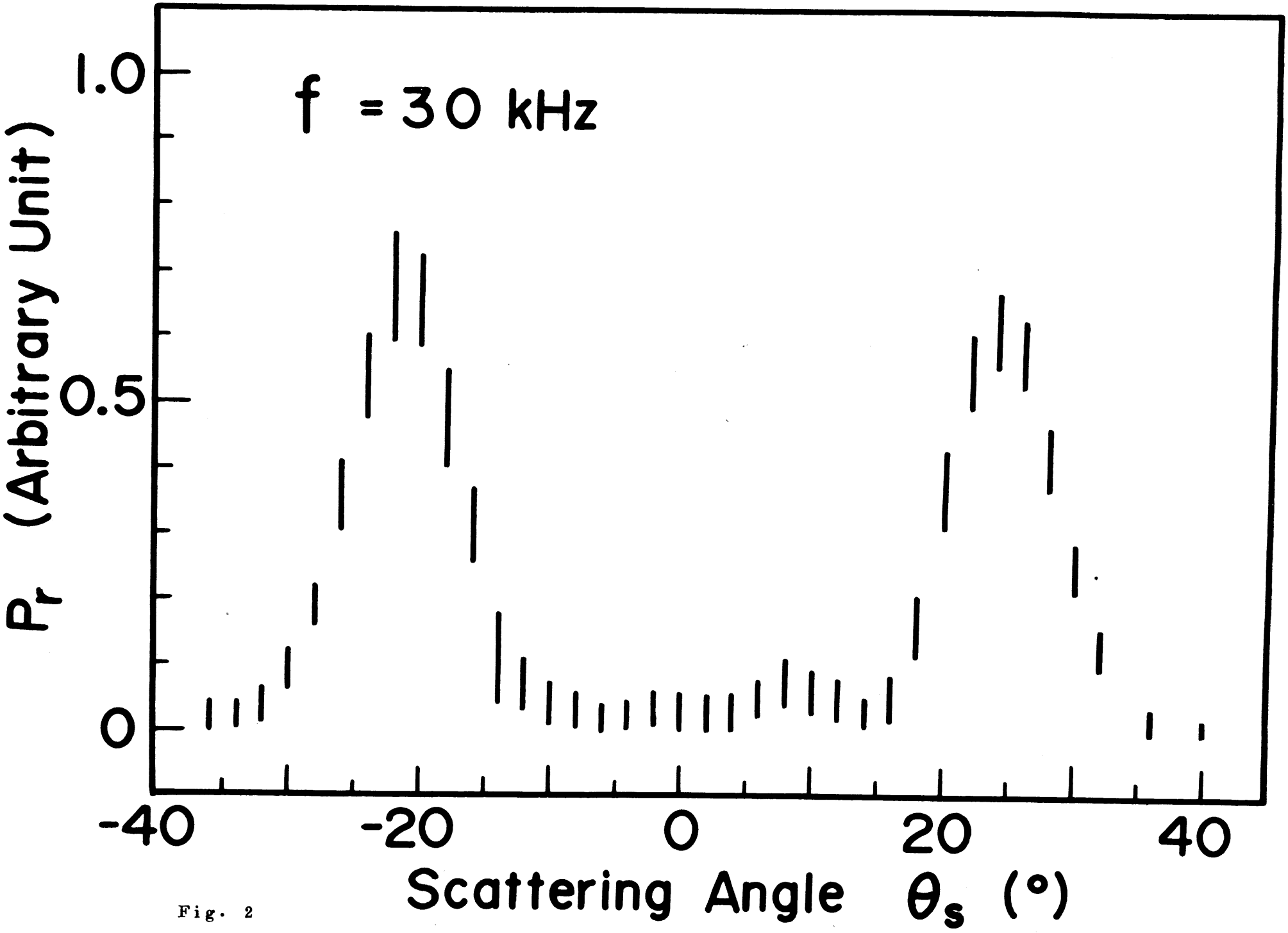
f = 30 kHz
1.0
0.5
0
P_r (Arbitrary Unit)
-40
-20
0
20
40
Scattering Angle θ_s (°)

Fig. 2

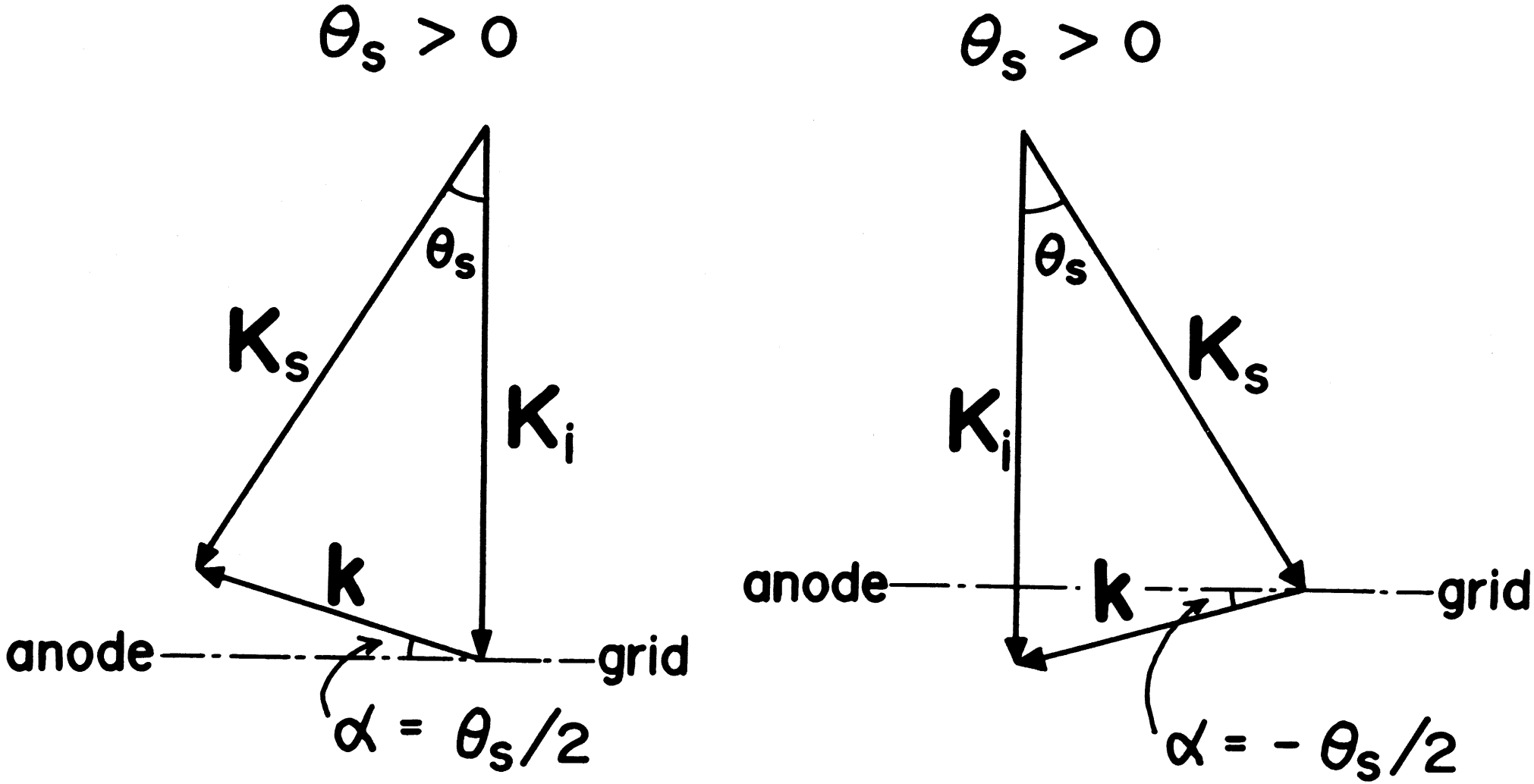

Fig. 8

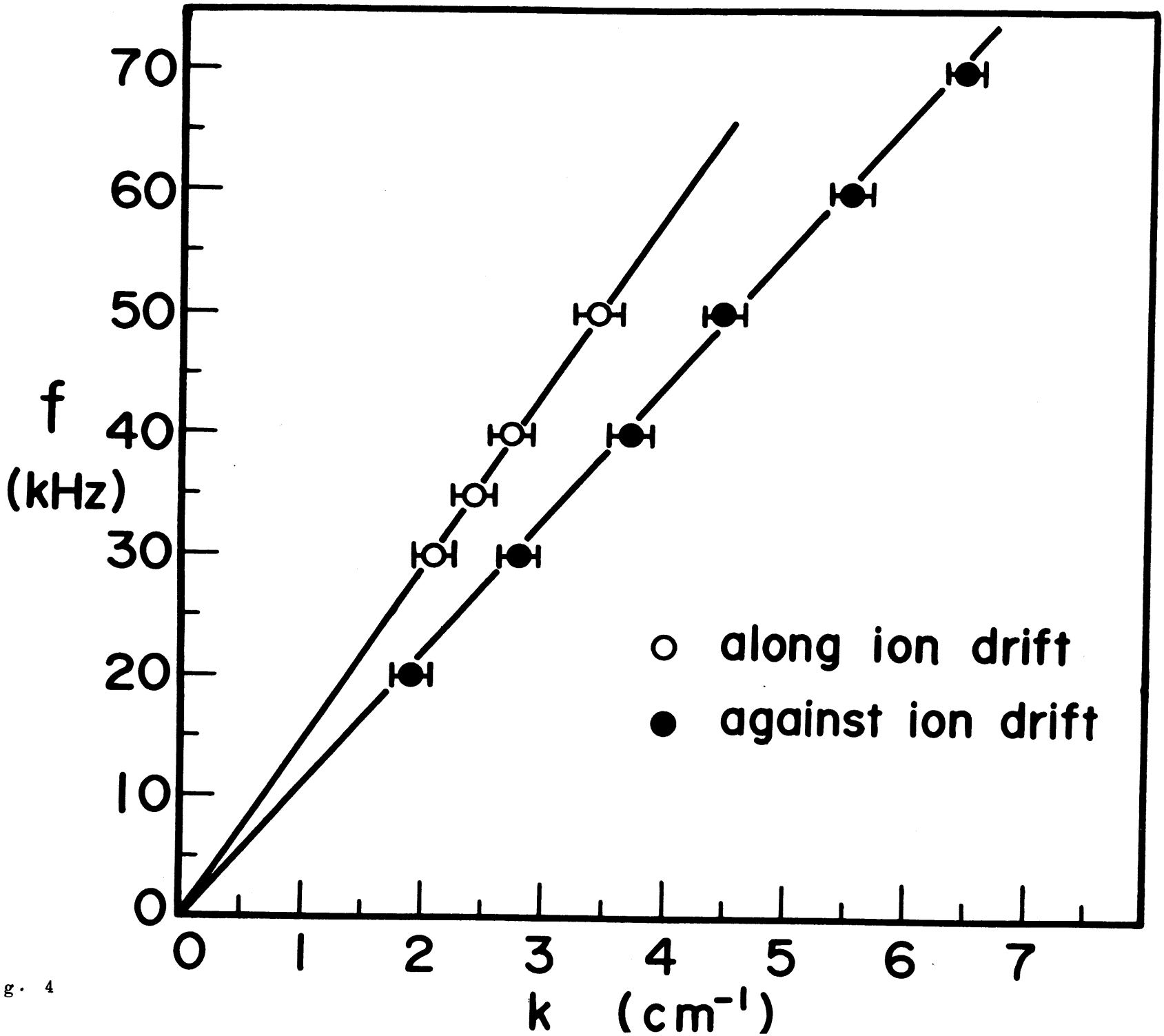
70
60
50
40
30
20
10
0
f
(kHz)
0
1
2
3
4
5
6
7
k (cm⁻¹)
along ion drift
against ion drift

Fig. 4

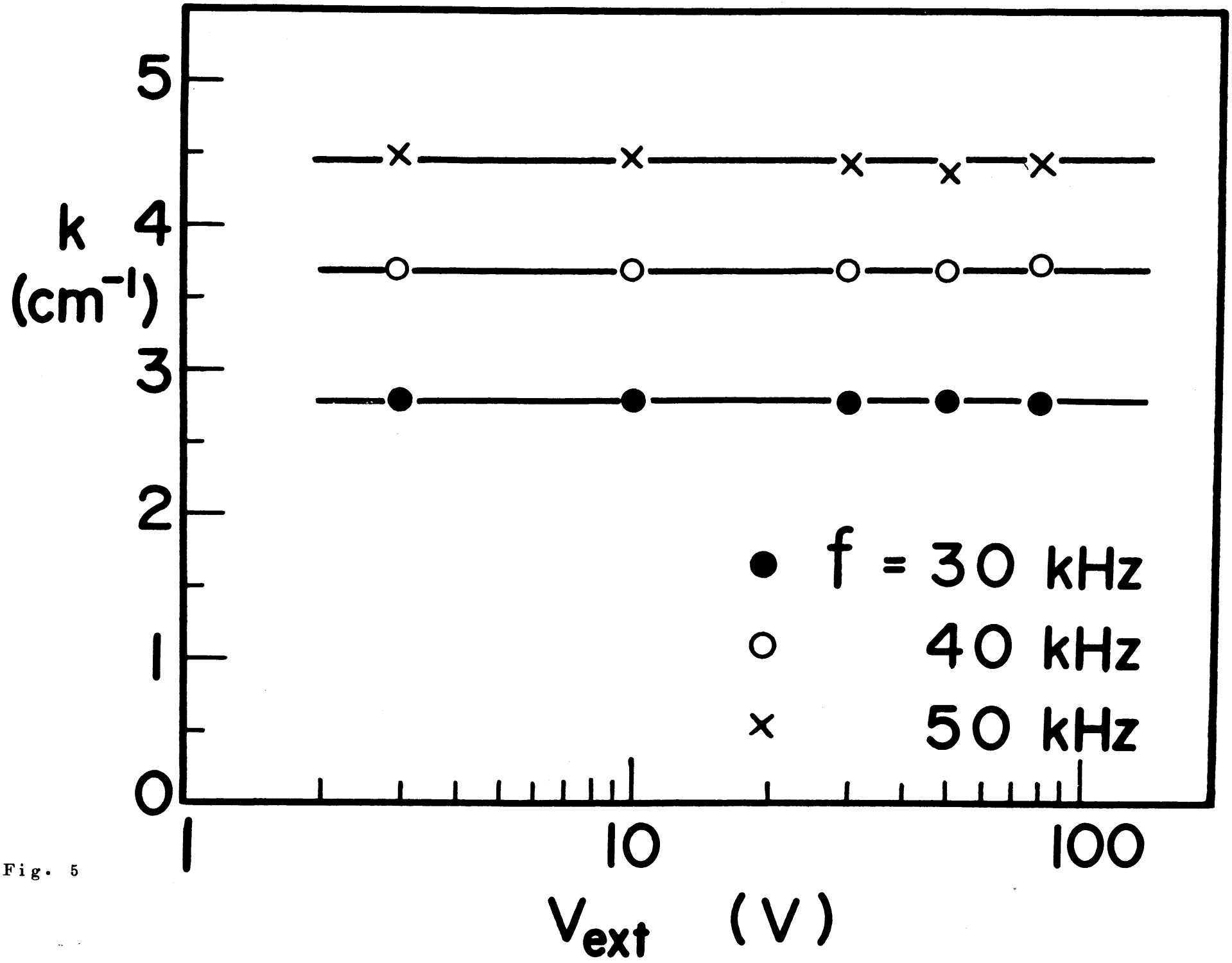

Fig. 5

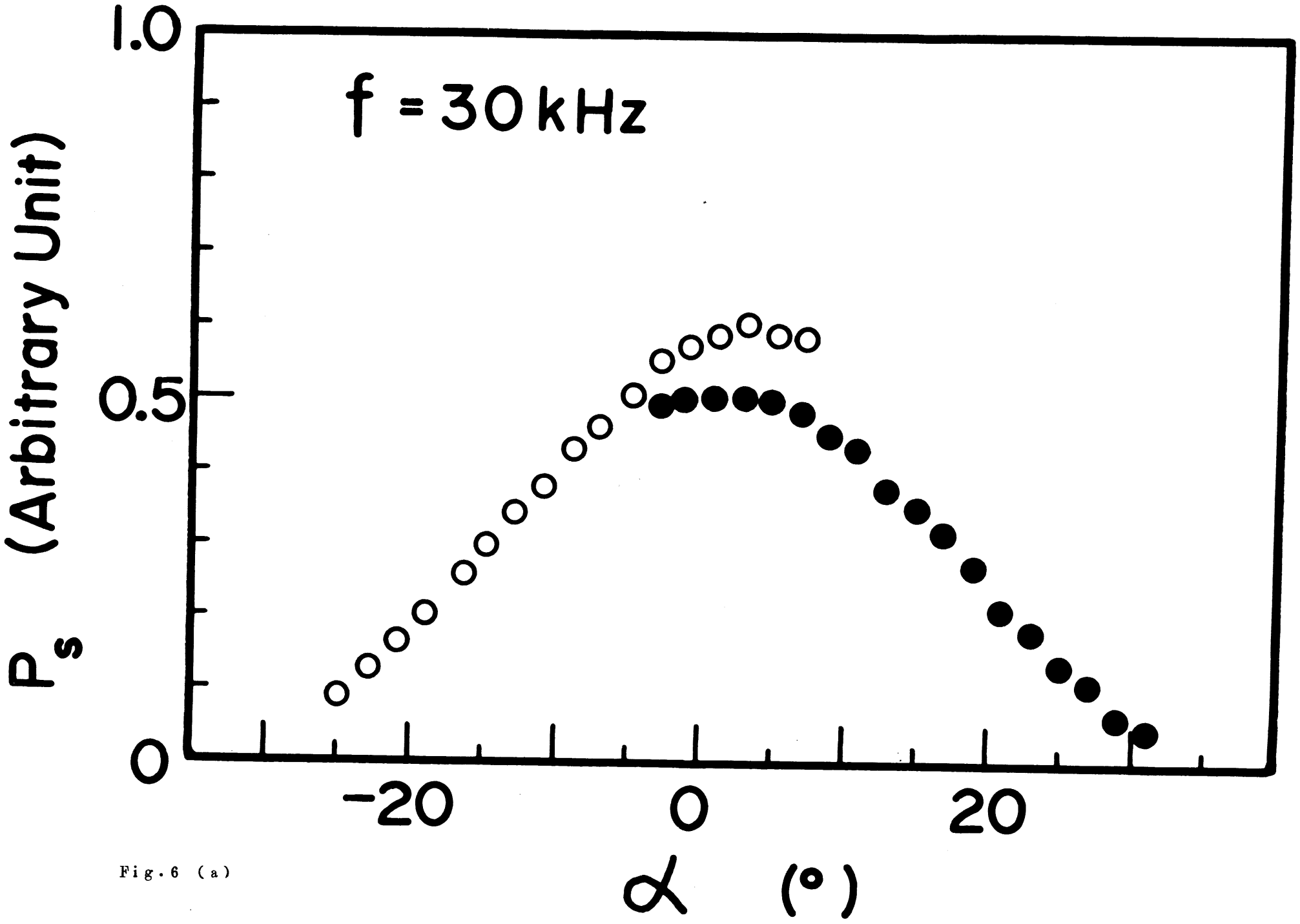

Fig. 6 (a)

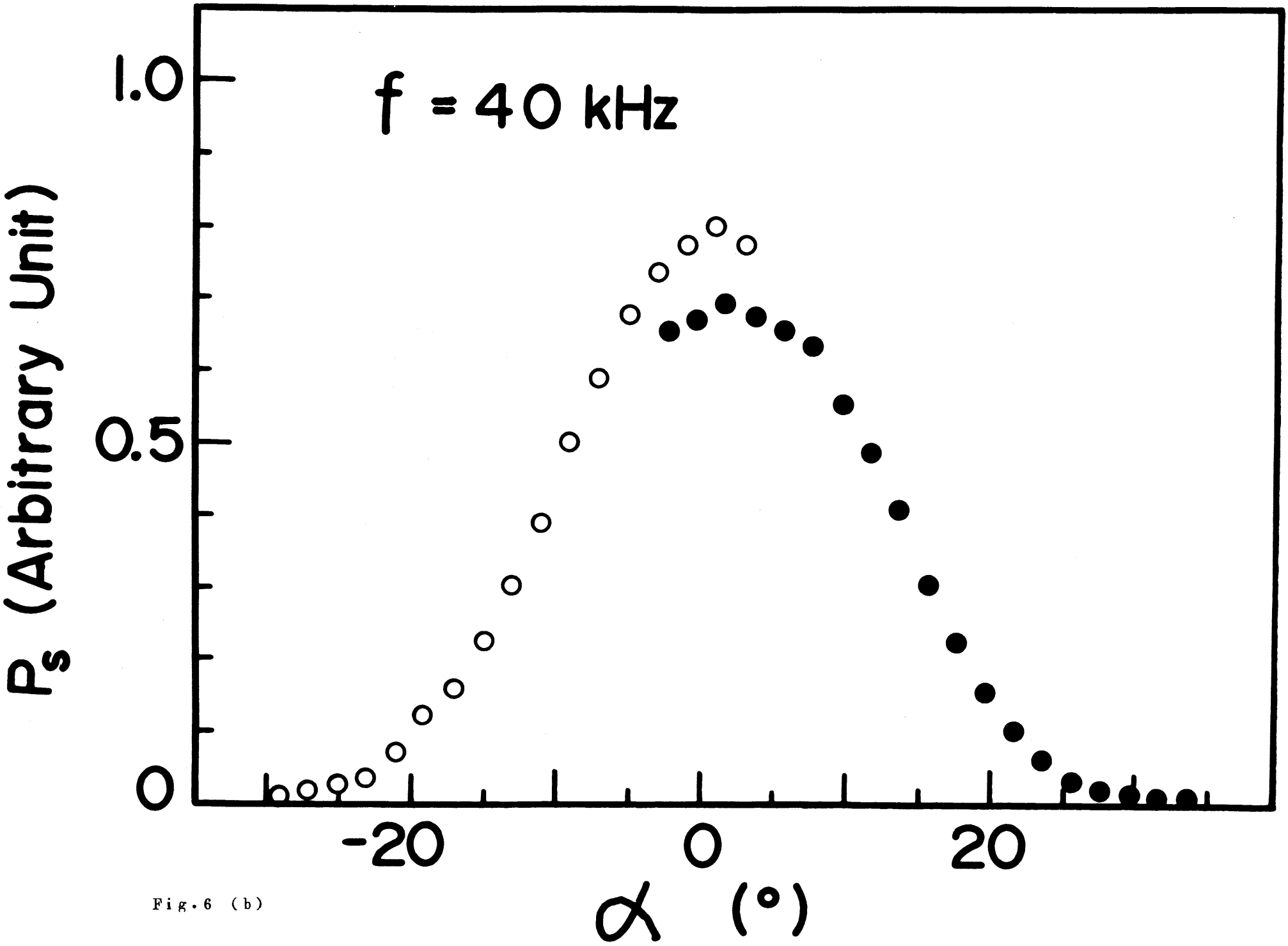

Fig.6 (b)

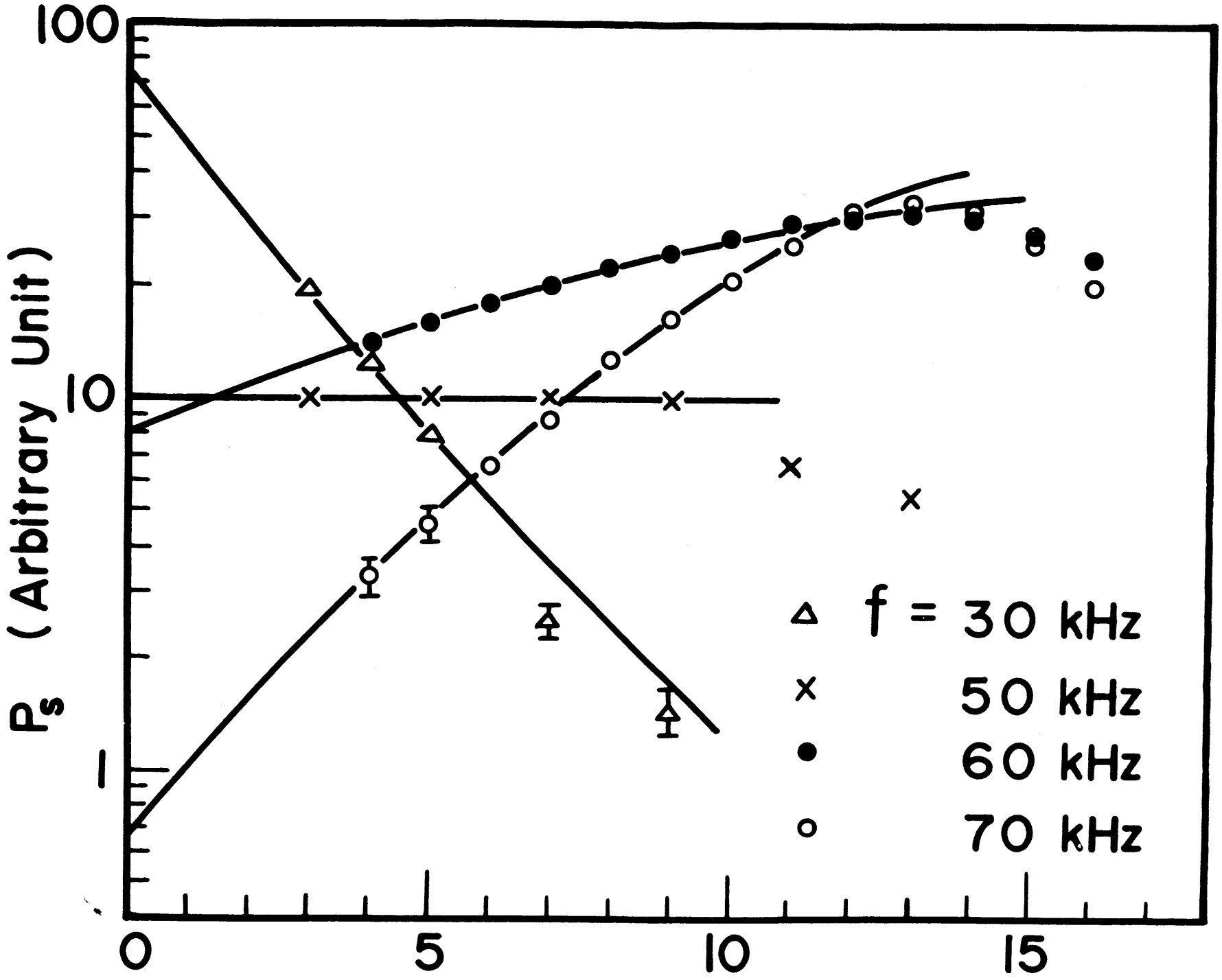

Fig. 7

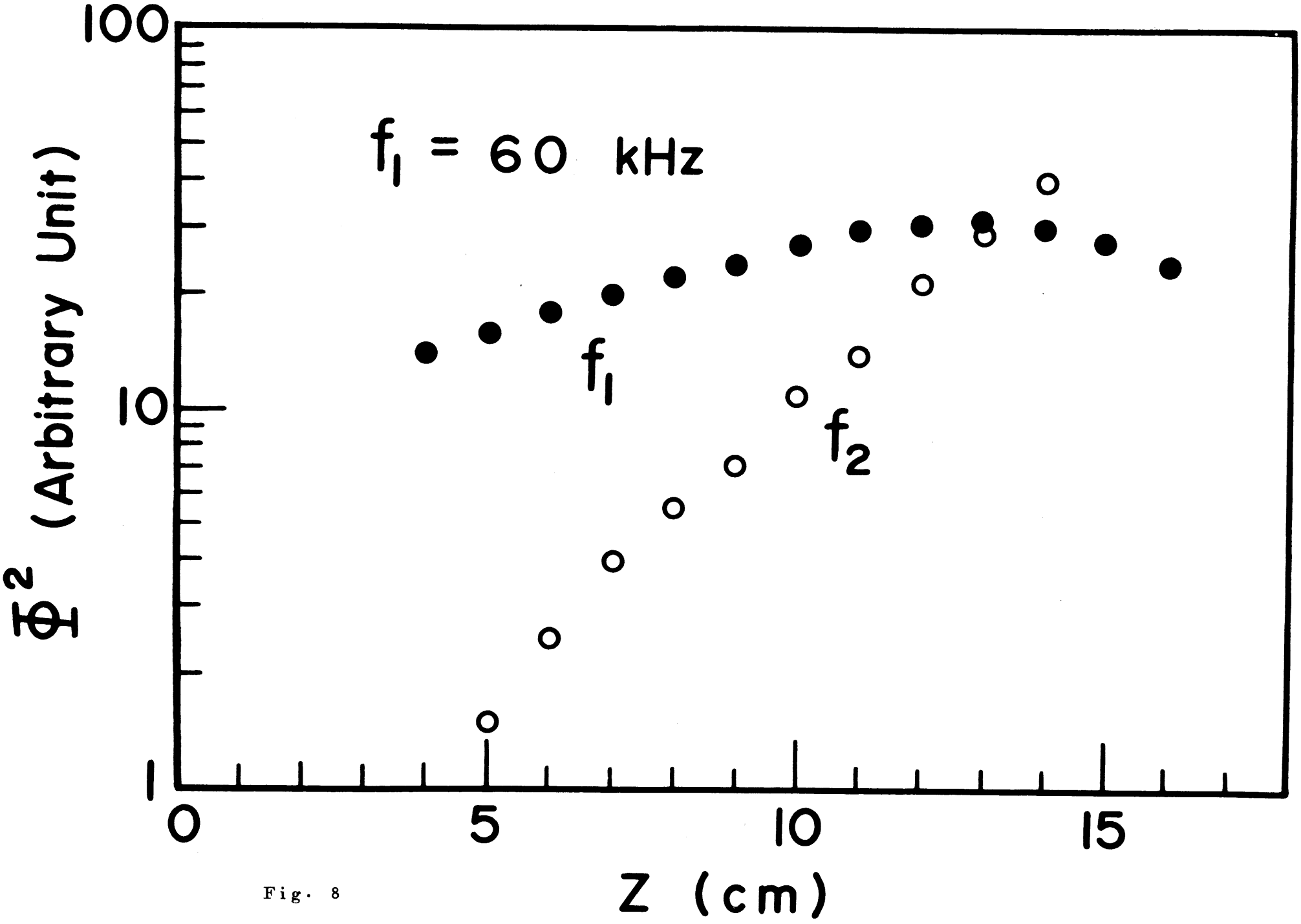

Fig. 8